Unscrambling Fluorophore Blinking for Comprehensive Cluster Detection via Photoactivated Localization Microscopy

Benedikt K. Rossboth*[$], Rene Platzer[§$], Eva Sevcsik*, Florian Baumgart*, Hannes Stockinger[§], Gerhard J. Schütz*, Johannes B. Huppa[§#] and Mario Brameshuber*[#]

*Institute of Applied Physics, TU Wien, Vienna, Austria;

[§] Institute for Hygiene and Applied Immunology, Center for Pathophysiology, Infectiology and Immunology, Medical University of Vienna, Vienna, Austria;

[$]both authors contributed equally

to whom correspondence should be addressed: brameshuber@iap.tuwien.ac.at or johannes.huppa@meduniwien.ac.at

GRAPHICAL ABSTRACT

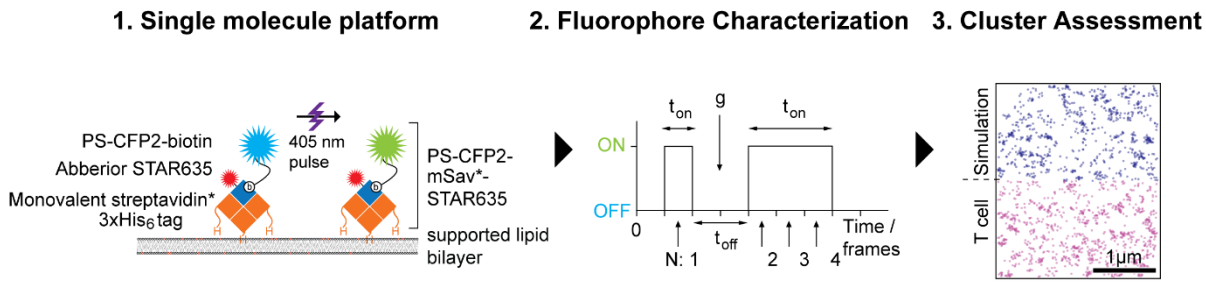

ABSTRACT

Determining nanoscale protein distribution via Photoactivated Localization Microscopy (PALM) mandates precise knowledge of the applied fluorophore's blinking properties to counteract overcounting artifacts distorting results. Here, we present a readily applicable methodology to determine, optimize and quantitatively account for the blinking behavior of any PALM-compatible fluorophore for maximal spatial resolution. Using a custom-designed platform we revealed complex blinking of single photoswitchable CFP2 (PS-CFP2) molecules with blinking cycles on time scales of several seconds, which we incorporated in our simulation-based analysis package to robustly evaluate individually recorded PS-CFP2 localization maps for molecular clustering.

INTRODUCTION

PALM is a single molecule localization microscopy (SMLM) technique devised to resolve structures below the diffraction limit. It relies on the stochastic switching of fluorophores between a blue-shifted fluorescent or dark state and a red-shifted or bright fluorescent state[1, 2]. Among photoswitchable fluorescent proteins utilized so far in PALM are Kaede[3], PAmCherry[4], Eos-based proteins[5], Dronpa[6] and variants of GFP such as photoactivatable GFP[7] (PA-GFP) and photoswitchable-CFP2[8, 9] (PS-CFP2) (reviewed in[10]). Photoswitching reduces the number of active fluorophores per recorded image by several orders of magnitude giving rise to well-separated single molecule signals, which are localizable with a precision primarily determined by the signal to noise ratio[11].

Numerous studies have addressed protein clustering within the plasma membrane using various photoswitchable FPs. However, the observation of repetitive on-off blinking challenged data interpretation, likely yielding false-positive cluster detection due to fluorophore overcounting[12]. Notably, mEos2 exhibited non-negligible light-induced fluorescence recovery from dark states[13] which was implicated in the recording of erroneous protein assemblies[12]. In contrast, blinking of PS-CFP2 was considered less pronounced[12, 14] and a high fraction of photoswitched PS-CFP2 molecules was reportedly bleached irreversibly upon high-powered 488 nm irradiation[15, 8]. Still, to this date the observation of reversible PS-CFP2 blinking cycles before terminal photobleaching[12, 14, 16, 17] has remained a challenge not only for quantitative PALM approaches[17-20] but also for more general conclusions relating to functionally relevant protein clustering and protein co-localization.

In this study we have devised and tested a widely applicable experimental and analytical platform to determine the blinking signature of photoswitchable and photoactivatable fluorophores for comprehensive protein cluster assessment in single cells. Employing commonly applied imaging conditions[15] we detected a single PS-CFP2 molecule, chosen here

as a representative photo-switchable fluorophore, on average 3.47 times with blinking cycle times in the order of seconds. Monte-Carlo simulated detections of randomly distributed PS-CFP2 molecules featuring PS-CFP2 blinking properties yielded considerable apparent clustering, which can, as we demonstrate, be quantitatively accounted for when evaluating PALM-generated localization maps. Our study highlights the need to reliably detect and experimentally optimize the blinking properties of photoswitchable fluorophores prior to their use in PALM. Our overall approach serves to precisely determine fluorophore-specific blinking parameters for reliable cluster evaluation of individually recorded localization maps.

Platform development to quantitate fluorophore blinking

We selected PS-CFP2 as a model fluorophore in view of its wide use in PALM and its reportedly low blinking tendency[12, 15]. To be able to determine fluorophore blinking properties with single molecule resolution, we site-specifically coupled recombinant PS-CFP2 via biotin modification to monovalent streptavidin (mSav*-3xHis_6, **Supplementary Fig. 1**), which was then anchored via its three histidine tags to 1,2-dioleoyl-sn-glycero-3-[(N-(5-amino-1-carboxypentyl)iminodiacetic acid)succinyl] (nickel salt) (DGS-NTA(Ni)) present together with 1,2-dipalmitoyl-sn-glycero-3-phosphocholine (DPPC) at a 1:200 ratio in a planar glass-supported lipid bilayer (SLB) (**Fig. 1A**). Specifics concerning the generation of mSav*-3xHis_6, its complex with PS-CFP2 and the protein-functionalized SLB are described in the Methods section and **Supplementary Fig. 1**.

This arrangement supported 2-dimensional imaging in total internal reflection (TIR) mode, as carried out in many PALM studies. The high melting temperature (41°C)[21] of the matrix lipid DPPC afforded continuous observation of SLB-immobilized fluorophores. Furthermore, the use of SLBs prevented non-specific fluorophore binding to the glass surface. False positive signals caused by trace amounts of (partly) hydrophobic buffer- or lipid-derived dyes[22]

intercalating with synthetic lipid bilayers were minimized by two-color co-localization between the fluorophore under investigation and the red-shifted dye Abberior STAR 635P (STAR635). The latter was site-specifically and quantitatively conjugated to an unpaired cysteine residue engineered within the biotin-binding subunit of mSav*-3xHis_6 (mSav*-STAR635, **Supplementary Fig. 1A and B**). A two-color data acquisition protocol with sequential excitation of both fluorophores was applied to select specifically for PS-CFP2 molecules co-localizing with mSav*-STAR635. **Fig. 1B** shows an overlay of images recorded in the red (mSav*-STAR635) color channel and localizations determined in the green (PS-CFP2) color channel. In control experiments conducted with SLBs solely decorated with mSav*-STAR635, only 2.6 ± 0.33 % (mean ± SEM) of signals in the green channel co-localized with mSav*-STAR635 visualized in the red channel, indicating a 38-fold reduction in false positive signals by applying the two-color colocalization protocol. Single molecule tracking of individual mSav*-STAR635 molecules testified to its quasi immobile state with a diffusion coefficient $D < 10^{-4}$ µm²/s (**Supplementary Fig. 2A**), rendering the platform suitable for the observation of the very same PS-CFP2 molecules over time-scales of seconds. **Fig. 1C** shows two representative intensity traces of PS-CFP2 recorded in a PALM experiment. Of note, emissive behavior varied substantially between different molecules and ranged from one-frame detections to repeated detections over multiple frames interrupted by several non-emissive gaps.

Figure 1

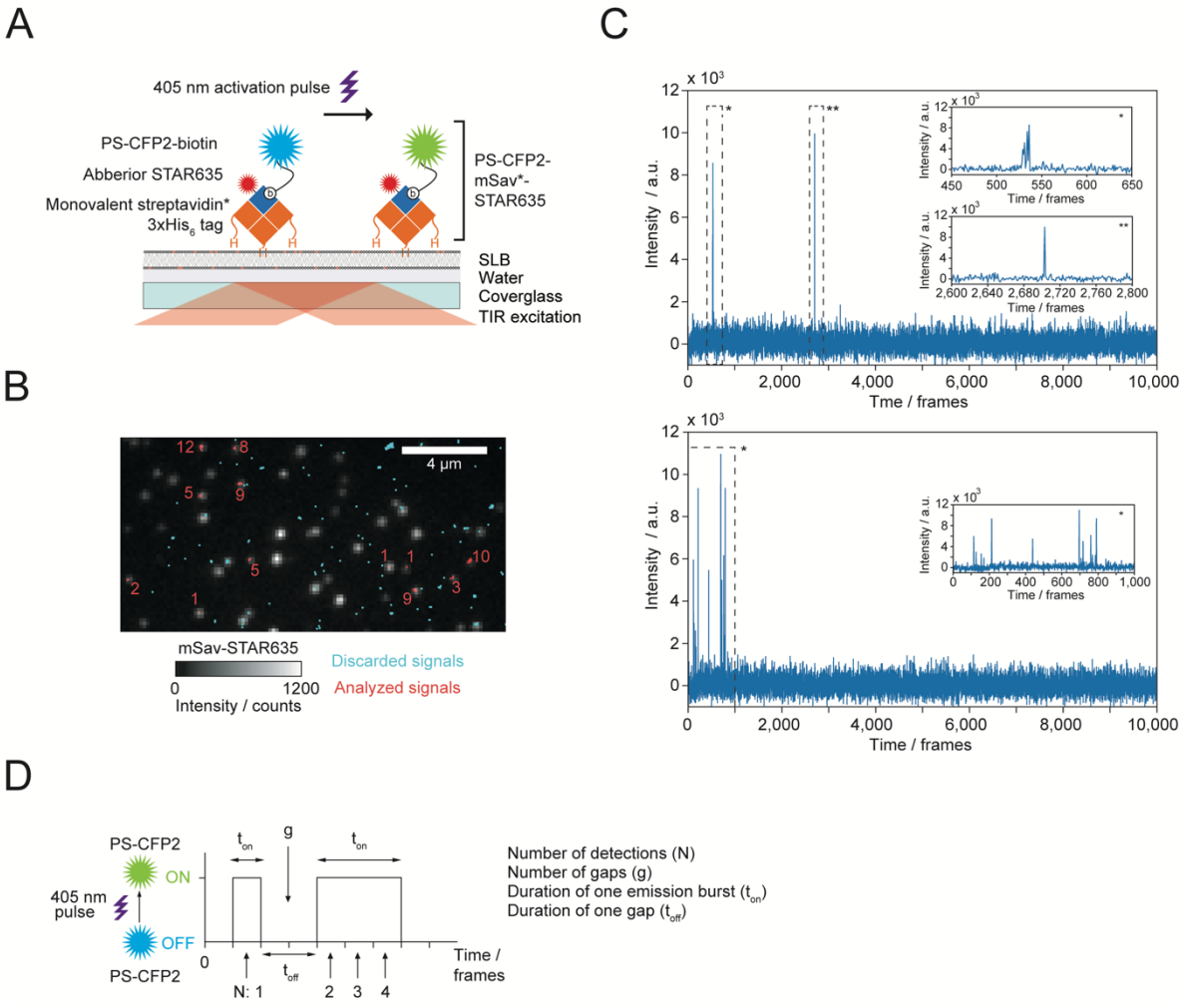

Figure 1. Imaging platform to quantitate blinking parameters of recombinant fluorescent proteins.

(**A**) PS-CFP2-mSav*-STAR635 conjugates were anchored to immobile SLBs containing 99.5% DPPC and 0.5% DGS-NTA(Ni). Single PS-CFP2 molecules were identified through colocalization with STAR635 in TIR mode, which allowed for precise acquisition of blink statistics on a single molecule level. (**B**) Two-color co-localization of STAR635 and PS-CFP2 enabled discrimination of false positive signals as shown in the images acquired for mSav*-STAR635 (monochrome color channel) and from consecutive PALM of single PS-CFP2 signals (red and cyan colored localizations). The total number of PS-CFP2 detections per analyzed signal are indicated in red. (**C**) Representative intensity traces acquired in 10,000 image frames for a single PS-CFP2 molecule exhibiting two bursts of localizations (upper panel) and a PS-CFP2 molecule exhibiting multiple bursts (lower panel). Inserts provide a higher temporal resolution of indicated traces. **(D)** Four parameters were extracted from single

molecule traces: (i) the total number of detections (***N***), (ii) the number of off-gaps (***g***) occurring within single traces, (iii) the duration of each emission burst (t_{on}), and (iv) the duration of each off-gap (t_{off}).

Determining PS-CFP2 blinking parameters

We analyzed the temporal emission patterns of single PS-CFP2 molecules with regard to four parameters affecting the interpretation of localization maps (**Fig. 1D**): (i) the total number of detections per molecule within the whole imaging sequence (***N***), (ii) the number of gaps within a single PS-CFP2 trace (***g***), (iii) the duration of each emissive state (t_{on}) and (iv) the duration of each gap (t_{off}). Of note, high values in N, g and t_{on} can in principle be adequately accounted for by simple merging strategies as long as values of t_{off} are low.

Fig. 2A shows the normalized histograms of all measured parameters for a total of 1080 analyzed PS-CFP2 molecules pooled from several experiments. When applying a 488 nm excitation power density of 3.0 kW cm^{-2} for 2 ms at a frame rate of 167 Hz, a single PS-CFP2 molecule was detected on average 3.47 times over the course of 10,000 frames (**Fig. 2A,** top panel). 65 % of molecules were detected more than once in the whole sequence; about 25 % of all molecules appeared more than 5 times with a maximum of 38 detections. A similar distribution was found for the normalized number of detected gaps, g, occurring within individual PS-CFP2 traces: 55% of PS-CFP2 molecules showed at least one gap; we observed a maximum amount of 31 gaps (**Fig. 2A,** insert top panel). The duration of emissive states was on average 1.3 frames (**Fig. 2A,** insert bottom panel). About 20% of detections resulted from signals localized in more than one consecutive frame, and only a minor fraction of 1% was detected in 5 or more consecutive frames. For molecules undergoing emission gaps, we further analyzed the distribution of t_{off} (**Fig. 2A,** bottom panel). While most molecules showed off-times shorter than 50 frames, the distribution featured an extended tail towards long off-times: 8% of the observed off-times ranged between 200 and ~9000 frames (not displayed for

improved graph clarity). The median gap duration was 10 frames, i.e. too high to be accounted for by simple event merging without losing information about real clustering.

Blinking properties of PS-CFP2 are affected by experimental conditions

To minimize diffusion during image acquisition in SMLM specimens are subjected in many cases to chemical fixation. After paraformaldehyde treatment (4 % PFA for 10 minutes) the average number of localizations per PS-CFP2 molecule increased to 4.88 and number of gaps per PS-CFP2 to 2.49 frames (**Fig. 2B**) while t_{on} (1.4 frames) and t_{off} (11 frames) remained largely unchanged compared to the experiment without PFA.

Super-resolution imaging protocols differ in applied acquisition rates, which typically range from 33 Hz[23] to 250 Hz[15], and also with regard to the excitation intensity of the imaging laser. Since the laser light employed for excitation drives at least in part transitions between bright and dark states, we sought to identify experimental settings which reduce overcounting.

To this end we examined the influence of lowering the excitation power 7.5-fold while keeping the energy density at the sample constant by increasing the illumination time accordingly. As shown in **Fig. 2C**, the mean number of detections per PS-CFP2 increased to 4.6, mainly due to a slightly increased number of gaps, *g*, per PS-CFP2 molecule and an increased t_{on}. The median duration of gaps decreased to 6 frames compared to the experiment involving the higher laser intensity. We next increased the excitation power density from 3.0 kW cm^{-2} to 15 kW cm^{-2} in an attempt to bleach every PS-CFP2 molecule within the first image frame after photoconversion. However, background fluorescence increased under these circumstances to levels which no longer allowed for a clear discrimination between localizations of single PS-CFP2 molecules and of background signals (**Supplementary Fig. 2B**).

In many applications, the fluorescent protein tag is exposed to the cytoplasm, which features a reducing redox potential attributable to reduced glutathione[24] (GSH) present in millimolar

concentrations. Since fluorophore bleaching and blinking is linked to oxidation of free radicals, we analyzed the emission characteristics of PS-CFP2 in the presence of 5 mM glutathione. The mean number of localizations per PS-CFP2 molecule dropped to 2.77 with a concomitant decrease in the number of gaps per PS-CFP2 molecule (**Fig. 2D**). While the duration of the emissive states remained unchanged compared to non-reducing conditions, the median duration of gaps increased from 10 to 18 frames.

A direct means of revealing single molecule blinking behavior is sorting the detections per molecule in ascending order and by normalizing the number of fluorophore localizations to the number of molecules recorded. In an ideal scenario, if a fluorophore is only detected once, this relation would yield a straight line with a slope of 1 (**Fig. 2E,** black dotted line). Each additional localization per molecule results in a deviation from this diagonal towards a higher number of detections per fluorophore. The plots obtained with PS-CFP2 (**Fig. 2E**) differ substantially from the diagonal; their maxima of about 2.8 (2 ms exposure at 3.0 kW cm^{-2}, 5 mM GSH; blue line), 3.5 (2 ms exposure at 3.0 kW cm^{-2}, black line), 4.5 (15 ms exposure at 0.4 kW cm^{-2}; red line), and 4.88 (2 ms exposure at 3.0 kW cm^{-2} and after PFA fixation; cyan line) are equivalent to the mean number of detections per PS-CFP2 molecule. Depending on the imaging conditions, 50% (blue line), 37% (black line), 32% (red line) or 26% (cyan line) of the PS-CFP2 molecules were detected only once, which, taken as a whole, accounted however for only 18%, 11%, 7%, or 5% of all detected signals. Hence, a total of 82-95% of PS-CFP2 detections arose from molecules which had appeared multiple times.

Figure 2

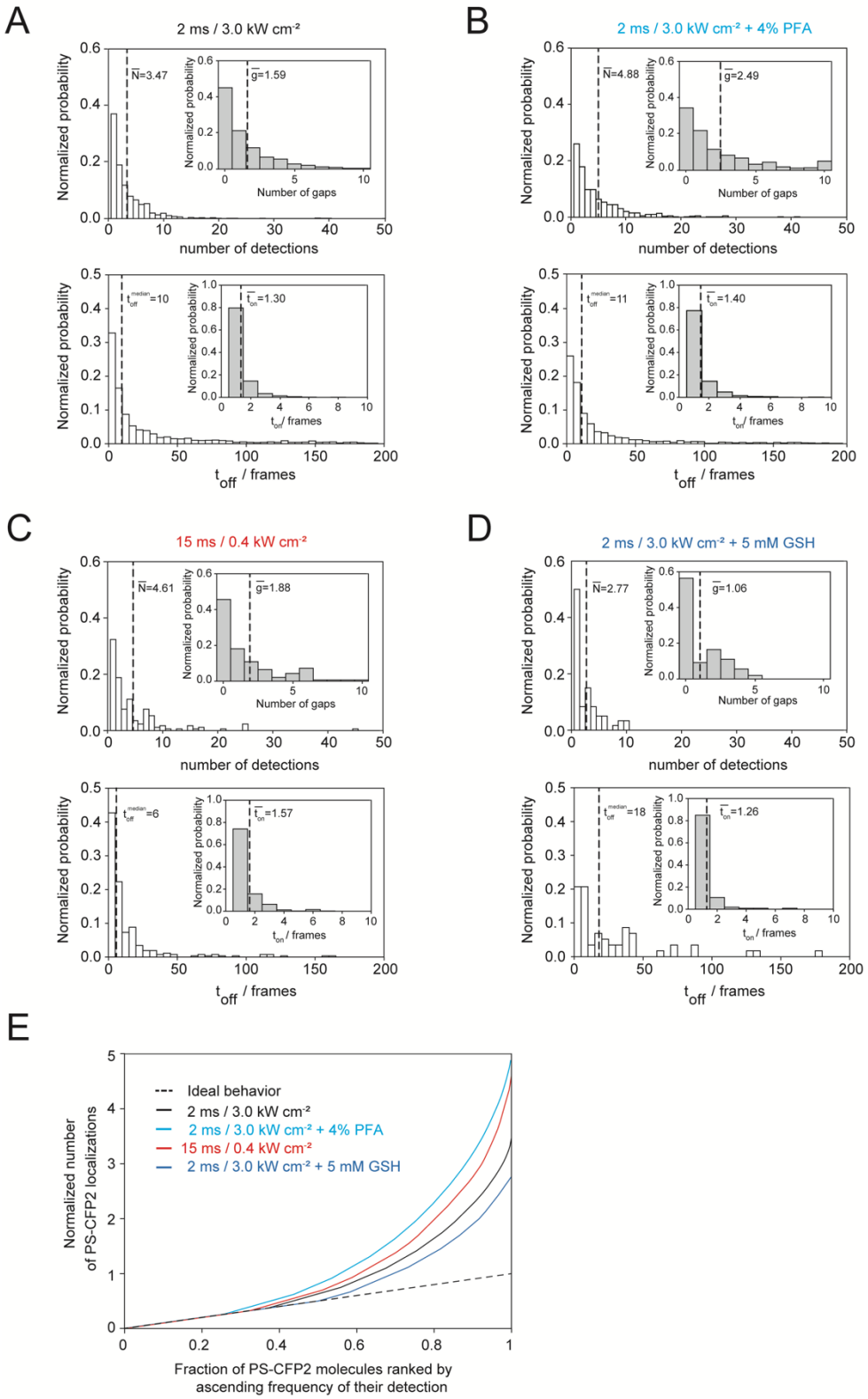

Figure 2. Detailed quantitation of PS-CFP2 blinking behavior.

(**A-D**) Normalized histograms illustrate four parameters described in (**Fig. 1D**) determined for four different experimental settings as is indicated. Numbers within the histograms indicate the

mean (-) or median value of the respective parameter. In total, 1080 (A), 580 (B), 61 (C), and 170 (D) PS-CFP2 molecules have been recorded. (**E**) Quantification of PS-CFP2 blinking: the numbers of PS-CFP2 detections per molecule were sorted in ascending order, and the respective fractions plotted against the normalized number of PS-CFP2 localizations. The black dotted diagonal indicates a hypothetical ideal scenario, in which each PS-CFP2 molecule gives rise to one single detection. Deviations from the diagonal indicate multiple detections per PS-CFP2 molecule.

Blinking distorts SMLM cluster maps

Reappearance of one and the same blinking molecule gives rise to false-positive protein clusters, especially when fluorophores are no longer mobile after chemical cell fixation. To illustrate how blinking affects data interpretation, we juxtaposed a randomized distribution of immobile fluorophores (**Fig. 3A**, blue) with its corresponding localization map, which was simulated based on the blinking characteristics of PS-CFP2 (determined at a power density of 3 kW cm^{-2} with 2 ms illumination time) (**Fig. 3A**, purple). The emergence of artificial clusters became evident already upon unaided inspection: a single blinking molecule gave rise to a cloud of localizations with a lateral extension in the order of their positional accuracy. Without PS-CFP2 blinking, Ripley's K analysis, which is commonly applied for cluster description in SMLM[25], yielded a constant value (**Fig. 3A**, bottom row), as would be expected for a random distribution. When implementing PS-CFP2-specific blinking, the normalized Ripley's K function resulted in a distinct peak indicating clusters of localizations. We next compared real protein clusters with their corresponding localization map as it manifested with PS-CFP2-specific blinking (at a power density of 3 kW cm^{-2} with 2 ms illumination). Both scenarios feature clearly discernible clusters affecting Ripley's K function (**Fig. 3A**). Importantly, based on Ripley's K analysis the random distribution of blinking fluorophores (**Fig. 3A**, lower left panel, purple) could not be discriminated from a clustered distribution of both non-blinking

and blinking fluorophores (**Fig. 3A**, lower right panel, purple and blue) without further knowledge of the fluorophores' blinking characteristics.

Classifying Ripley's K functions to distinguish molecular clustering from random distributions

Qualitative comparison of Ripley's K functions derived from randomized and clustered scenarios of blinking PS-CFP2 molecules (**Fig. 3A**, lower left and right, purple) yielded clear disparities, in particular with regard to their respective maximum values. Hence, with precise knowledge of the blinking properties, a purely random distribution is quantitatively distinguishable from a clustered distribution through comparison of the respective Ripley's K function maxima (**Fig. 3B**). To assess the sensitivity of our combined approach, we charted PS-CFP2 nanoclustering scenarios, which were no longer resolvable by means of Ripley's K function analysis and hence would be classified as random distributions (**Fig. 3C**). Only if clusters comprised 20% or fewer than 20% of all recordable molecules, they evaded detection. The addition of 4% PFA did not change the sensitivity in detecting protein clusters (**Fig. 3C**, top right). An even larger number of scenarios could in principle be determined when imaging in the presence of GSH (**Fig. 3C**, bottom right), while fewer clustering scenarios were resolvable when applying prolonged illumination times (**Fig. 3C**, bottom left).

For method validation we assessed the cell surface distribution of both T-cell antigen receptor (TCR)- associated CD3ζ fused to PS-CFP2 (CD3ζ-PS-CFP2) and the integrin LFA-1 decorated with a biotinylated LFA-1α chain-reactive antibody for detection via mSav*-cc-PS-CFP2. T-cells, either placed on SLBs presenting the adhesion molecule ICAM-1 or on fibronectin-coated glass-slides, were subjected to chemical fixation followed by PALM analysis applying the same experimental settings employed to determine PS-CFP2 blinking properties (i.e. 2 ms exposure at 3.0 kW cm^{-2}, PFA-treatment; refer to Methods section for details). As shown in

Fig. 3D, (left and right panel, red) localization maps of both CD3ξ and LFA-1 featured clearly discernible clusters. However, comparison of the Ripley's K function resulting from the CD3ξ-PS-CFP2 PALM recording with those calculated from random distributions of simulated entities featuring PS-CFP2 blinking properties (**Fig. 3D**, left panel, blue) yielded no significant differences (**Fig. 3D**, left bottom panel), confirming previous results derived from a label density variation approach[26]. In contrast and consistent with earlier observations, antibody-labeled LFA-1 detected with mSav*-cc-PS-CFP2 gave rise to localization clusters which could no longer be explained by overcounting only and which must hence have originated from LFA-1 nano-clustering[26, 27] (**Fig. 3D**, right).

Figure 3

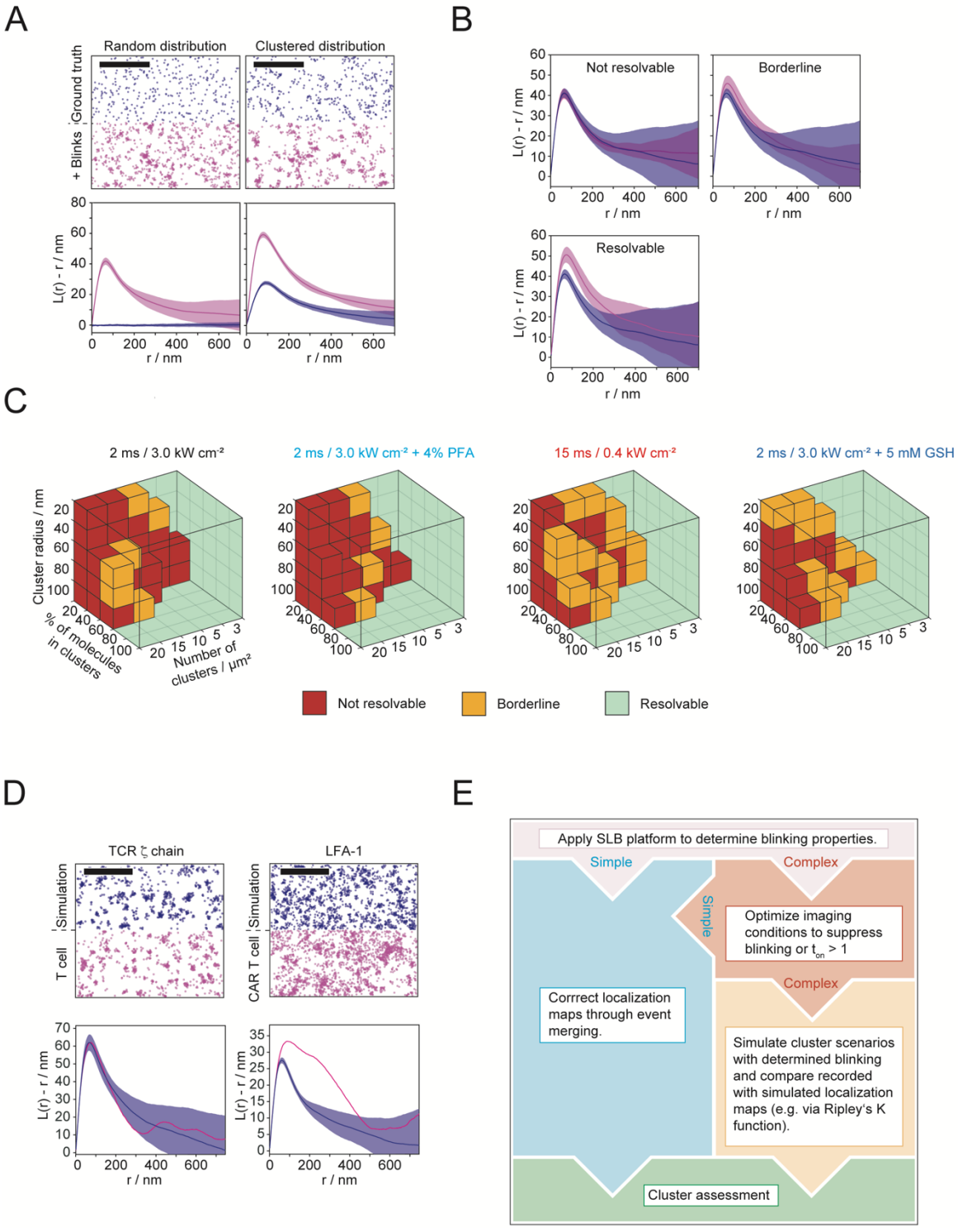

Figure 3. Monte Carlo simulation-based approach to discriminate random from clustered molecular distributions of fluorophores featuring complex blinking parameters.

(**A**) Fluorophore blinking affects Ripley's K functions: Top: We simulated super-resolution images without blinking (blue) and with experimentally derived blinking parameters of PS-

CFP2 (red) by distributing molecular positions randomly (left panel) or clustered (right panel, cluster radius: 60 nm, density of clusters: 20 cluster/µm² and 80% of molecules within clusters) at a density of 70 molecules/µm². Bottom: Ripley's K analysis of 15 simulations (mean ± SD). (**B**) Comparison of Ripley's K functions derived from super-resolution images simulated under different clustering scenarios: cluster scenarios are classified as not resolvable, if mean values are within the respective confidence interval (top left), as borderline, if confidence intervals overlap at the maximum of Ripley's K function, but the mean values are not within the intervals and as resolvable (top right), if confidence intervals do not overlap at the maximum of Ripley's K function (bottom left). (**C**) Sensitivity of Ripley's K analysis in detecting clustering scenarios. Ripley's K functions were determined from Monte Carlo simulations of nanoclusters with a cluster radius of 20, 40, 60 or 100 nm, a fraction between 20% and 100% of molecules residing inside clusters, 3, 5, 10, 15 and 20 clusters per µm², an average molecular density of 70 molecules μm^{-2} and the experimentally determined blinking statistics of PS-CFP2 determined under indicated imaging conditions. Functions were compared to those calculated from random distributions and categorized as described in (B). **(D)** Classification of CD3ζ and LFA-1 distribution on fixed T cells: Top: Randomized distributions superimposed with experimentally determined blinking parameters of PS-CFP2 were simulated at densities of 86 (CD3ζ) and 145 (LFA-1) molecules μm^{-2} (blue) for comparison with localization maps derived from PALM experiments involving CD3ξ-PS-CFP2 and anti-LFA-1-biotin-mSav*-cc-PS-CFP2* (red). Bottom: Ripley's K functions of CD3ξ-PS-CFP2 and anti-LFA-1-biotin-mSav*-cc-PS-CFP2* (red) were compared to Ripley's K functions derived from 10 simulations of randomized distributions with corresponding molecular densities (blue, mean ± SD). While the distribution of CD3ζ could not be discriminated against a random scenario, LFA-1 distribution deviated significantly. (**E**) Flow chart for cluster assessment. Scale bars 1 µm.

DISCUSSION

Unambiguous detection of one and the same single fluorescent dye reveals blinking behavior of photo-switchable fluorophores in all its complexity under experimental conditions which are in essence identical to those employed in PALM imaging experiments. For proof of principle we opted to quantitate the blinking of PS-CFP2, which had previously been described as less prone to blinking[15] and hence constituted an interesting candidate for SMLM. Unlike previous qualitative assessments, we showed that single PS-CFP2 molecules undergo several cycles of emissive states on time scales of several seconds, which are typical for super-resolution experiments. Only 26- 50% of all molecules gave rise to exactly one localization, while the remaining 50-74% fluorophores were represented in the data set at least twice. We consider it very likely that blinking of other photo-switchable fluorophores commonly employed in PALM studies will drastically affect cluster interpretation if not accounted for in a manner presented here.

Of critical importance for PALM data correction and subsequent interpretation is the finding that the distribution of blinks per molecule does not follow a simple geometric function as was previously described for single mEOS2 proteins[19,29]. Furthermore, simple merging procedures, which are based on time stamping, fail to account for outliers with excessive blinking. As a consequence and as shown in this study, cluster analysis based solely on the use of normalized Ripley's K functions [25] or other cluster assessment tools cannot provide the means to distinguish between a random distribution of fluorophores, which blink like PS-CFP2, and a clustered non-random distribution of non-blinking molecules. Importantly, high-powered fluorophore excitation (at 15 kW cm^{-2}) aimed to suppress PS-CFP2 blinking altogether did not provide a solution to the problem due to resulting high number of unspecific signals undistinguishable from true PS-CFP2 detections. This was mainly because background fluorescence increased with rising excitation power density while fluorophore emission signals

remained constant due to photon saturation. Given similar spectroscopic properties, we expect to observe similar behavior for most if not all PALM-compatible fluorescent proteins.

Detailed fluorophore characterization prior to conducting SMLM with the use of mEos2 [19, 29-32], PA-GFP and PA-mCherry1 [33] was previously shown instrumental for quantitative readout and also for maximally achievable resolution [34]. As is outlined in **Fig. 3E**, we arrived at the maximal sensitivity of PALM-based cluster detection by (i) precisely determining blinking statistics for given experimental conditions, (ii) comparing Ripley's K functions for simulated clustering scenarios and through (iii) variation of cluster distribution parameters and subsequent classification. Hence, our SLB-based experimental platform serves primarily the means to minimize blinking in PALM experiments through identification of suitable fluorophores and adequate imaging conditions, which give rise to low t_{off} values, as this would render simple merging and time stamping procedures sufficient to circumvent overcounting artefacts. If this cannot be achieved as showcased here for PS-CFP2, we provide an alternative strategy involving quantitative Ripley's K analysis-based comparison of PALM derived localization maps and of simulated event distributions derived from defined clustering scenarios and blinking properties. Of note, the presented, most straight-forward classification via Ripley's K function can be supplemented by other cluster assessment tools, which have been recently reviewed in view of their capability to distinguish random from clustered molecular appearances [35].

Knowledge of how imaging conditions affect fluorophore blinking may well be the deciding factor when probing for subtle differences in clustering between individual samples. Of note, when aiming for meaningful 2- color PALM-based co-localization there is no viable alternative to identifying photoswitchable fluorophores featuring simple blinking behavior. The experimental approach described herein affords maximal control and thus most direct means to achieve this. It may furthermore serve to improve the sensitivity of existing cluster

assessment strategies such as fluorophore dilution and other measures to counteract artefacts resulting from fluorophore overcounting[26,29].

MATERIALS AND METHODS

Animal model and ethical compliance statement

5c.c7 αβ TCR-transgenic mice bred onto the B10.A background were a kind gift from Björn Lillemeier (Salk Institute, USA). Animal husbandry, breeding and sacrifice for T cell isolation were evaluated by the ethics committees of the Medical University of Vienna and approved by the Federal Ministry of Science, Research and Economy, BMWFW (BMWFW-66.009/0378-WF/V/3b/2016). All animal related procedures were performed in accordance with the Austrian law (Federal Ministry for Science and Research, Vienna, Austria), the guidelines of the ethics committee of the Medical University of Vienna and the guidelines of the Federation of Laboratory Animal Science Associations (FELASA). Male and female mice 8-12 weeks of age were randomly selected for euthanasia, which was followed by the isolation of T cells from lymph nodes and spleen.

Tissue culture

T cells isolated from lymph nodes of 5c.c7 αβ TCR transgenic mice were pulsed with 1 µM C18 reverse-phase HPLC–purified MCC 88-103 peptide (sequence: ANERADLIAYLKQATK, T-cell epitope underlined; Elim Biopharmaceuticals) and 50 U ml^{-1} IL-2 (eBioscience) for 7 days [30]. T cells were cultured at 37°C in 1640 RPMI media (Life technologies) supplemented with 10% FCS (Merck), 100 µg ml^{-1} penicillin (Life technologies), 100 µg ml^{-1} streptomycin (Life technologies), 2 mM L-glutamine (Life technologies), 0.1 mM non-essential amino acids (Lonza), 1 mM sodium pyruvate (Life technologies) and 50 µM β-mercaptoethanol (Life technologies) in an atmosphere containing 5% CO2.

For retrovirus production we transfected the Phoenix packaging cell line with pIB2-CD3ξ-PS-CFP2 and the helper plasmid pcL-eco one day after T cell isolation. Three days after isolation,

we subjected T cells to virus-containing supernatant from the Phoenix culture, 10 µg/ml polybrene (Sigma) and 50 U/ml IL-2 (Sigma) followed by spin-infection for 90 minutes at 30°C and 1000g. Addition of 10 µg/ml blasticidin (Sigma) 24 hours after spin infection ensured selection of transduced cells. Dead cells were removed on day 6 after T cell isolation through density-dependent gradient centrifugation (Histopaque 1119, Sigma) and experiments were conducted between day 7 and day 9 after isolation.

Human CAR T cells were a kind gift of Michael Hudecek (University Clinics Würzburg, Germany). CAR T cells were cultured at 37°C and 5 % CO_2 in CAR T cell medium, i.e. 1640 RPMI media (Life technologies) supplemented with 10 % human serum, 100 µg ml^{-1} penicillin (Life technologies), 100 µg ml^{-1} streptomycin (Life technologies), 2 mM L-glutamine (GlutaMAX™ Supplement, Gibco), 25 mM HEPES and 50 µM β-mercaptoethanol (Life technologies). K562 feeder cells expressing the cognate CAR antigen ROR1 (K562-ROR1) were used to stimulate CAR T cells and maintained in 1640 RPMI media (Life technologies) supplemented with 10 % FCS (Merck), 100 µg ml^{-1} penicillin (Life technologies), 100 µg ml^{-1} streptomycin (Life technologies), 2 mM L-glutamine (Life technologies). One day prior to expansion, CAR T cells were thawed after storage in liquid nitrogen and allowed to recover overnight in CAR T cell medium supplemented with 10 U ml^{-1} IL-2. On the first day of the 8-day expansion protocol (day 1), 1 x 10^6 T cells and 5 x 10^6 feeder cells, which had been irradiated with 80 Gy, were pooled in 15 ml CAR T cell medium in a T25 flask, which was left in the vertical position. On day 2, IL-2 was added to a final concentration of 50 U ml^{-1}. Starting from the day 3, 7.5 ml conditioned medium was substituted every second day with 7.5 ml of fresh CAR T cell medium supplemented with 100 U ml^{-1} IL-2. Experiments were performed between day 8 and 11 and at least 12 hours after media exchange.

Protein expression, refolding and preparation of imaging tools

Monomeric photoswitchable cyan fluorescence protein 2 (PS-CFP2, Evrogen) was C-terminally equipped with an AVI-tag (GLNDIFEAQKIEWHE) for site-specific biotinylation via the BirA ligase (Avidity) followed by a 3C protease cleavable (LEVLFQGP) 12 x histidine (12xHis) tag (**Supplementary Fig. 3**). The PS-CFP2-AVI-3C-12xHis construct was synthesized by Eurofins MWG Operon and shuttled into the pet21a (+) vector using the restriction enzymes NdeI and HindIII. Optionally, we substituted a serine for an unpaired cysteine in the linker sequence between the AVI-tag and 3C protease cleavage site (**see Supplementary Fig. 3**) to create a target site for site-specific conjugation via click chemistry (PS-CFP2*). Both, PS-CFP2-AVI-3C-12xHis and PSCFP2*-AVI-3C-12xHis were expressed as soluble proteins in *E. coli* (BL-21) for 3 h at 30 °C. Bacterial cells were processed via ultrasound, subjected to ice-cold nickel binding buffer containing 50 mM Tris-HCl pH 8.0, 300 mM NaCl (Sigma), 10 mM imidazole (Sigma), 1 mM PMSF (Merck) and a protease inhibitor cocktail (complete™, Roche) and subjected to centrifugation. The supernatant was filtered (Filtropur S 0.2 µm, Sarstedt) and subjected to Ni-NTA based affinity chromatography (QIAGEN). Eluted protein was further purified by anion exchange chromatography (MonoQ 5/50 GE Healthcare Life Sciences) and gel filtration (Superdex-200 10/300 GE Healthcare Life Sciences). Fractions containing monomeric PS-CFP2 were concentrated with Amicon Ultra-4 centrifugal filters (10 kDa cut-off, Merck) and the maturation state of the fluorescent PS-CFP2 protein was verified via protein absorbance at 280 nm and 400 nm. Monomeric PS-CFP2 was site-specifically biotinylated using the BirA ligase (Avidity) to obtain the molecular probe biotin-PS-CFP2. The 12xHis-tag was removed by overnight digestion with 3C protease (GE Healthcare Life Sciences) followed by a purification step with Ni-NTA agarose (QIAGEN) to separate the cleaved biotin-PS-CFP2 from 3C protease (His-tagged) and unprocessed biotin-PS-CFP2-12xHis. The unbound protein fraction containing biotin-PS-CFP2 was again purified

via gel filtration (Superdex-200 10/300 GE Healthcare Life Sciences). The monomeric biotin-PS-CFP2 was stored in 1 x PBS at -80 °C.

After refolding and purification, fractions containing monomeric PSCFP2*-AVI-3C-12xHis were concentrated using Amicon Ultra-4 centrifugal filters (10 kDa cut-off, Merck) in the presence of 100 µM Tris(2-carboxyethyl)phosphine (TCEP, Thermo Fisher Scientific). Monomeric PS-CFP2*-AVI-3C-12xHis was site-specifically conjugated with 6-Methyl-Tetrazine-PEG4-Maleimide (Jena Bioscience) to arrive at PS-CFP2*-tetrazine and further processed as described below.

The cysteine mutant of the monovalent streptavidin (mSav*) was prepared with some adaptions as described[31, 32]. The pET21a (+) vectors encoding "alive" (i.e. biotin binding) and "dead" (i.e. biotin non-binding) streptavidin subunits were kindly provided by Alice Ting (Stanford University, USA). The sequence of the "dead" subunit was C-terminally extended with a 6 x histidine tag for attachment to lipid bilayers containing 18:1 DGS-NTA(Ni) (**Supplementary Fig. 4**). In the "alive" subunit, we substituted the 6 x histidine tag with a cleavable 6 x glutamate tag to allow for purification via anion exchange chromatography (Mono Q 5/50 GL) preceded by a recognition site of the 3C protease for optional removal of the tag. Furthermore, we substituted an alanine for a cysteine residue at position 106 (A106C) in the "alive" subunit, to produce a monovalent streptavidin that could be site-specifically conjugated to maleimide-linked fluorescent dyes (mSav*) (**Supplementary Fig. 5**). Both, "alive" and "dead" streptavidin subunits were expressed in *E. coli* (BL-21) for 4 h at 37 °C and refolded from inclusion bodies as described[32]. After refolding, the streptavidin tetramer mixture was concentrated in a stirred ultrafiltration cell (10 kDa cut-off, Merck). Further concentration and buffer exchange to 20 mM Tris-HCl pH 8.0 were carried out with Amicon Ultra-4 centrifugal filters (10 kDa cut-off, Merck). The mixture of tetramers was then purified by anion exchange chromatography (MonoQ 5/50 GE Healthcare Life Sciences) using a column gradient from 0.1

to 0.4 M NaCl. Monovalent streptavidin (mSav*) was eluted with 0.22 M NaCl, concentrated again (Amicon Ultra-4 centrifugal filters, 10 kDa cut off) and further purified via gel filtration (Superdex-200 10/300 GE Healthcare Life Sciences). The protein was either stored at -80 °C in 1 x PBS or site-specifically labeled with Abberior STAR 635P maleimide (Abberior) according to the manufacturer´s protocol and in the presence of 100 µM Tris(2-carboxyethyl)phosphine (TCEP, Thermo Fisher Scientific). To remove excess dye, STAR635-conjugated mSav* was purified by gel filtration using Superdex 75 (Superdex 75, 10/300 GL, GE Healthcare Life Sciences). Fractions containing monomeric mSav*-STAR635 were concentrated with Amicon Ultra-4 centrifugal filters (10 kDa cut off, Merck) to arrive at a protein concentration of ~1 mg ml^{-1}. The mSav*-STAR635 exhibited a protein to dye ratio of 1.0 as determined by spectrophotometry at 280 nm and 638 nm.

To arrive at a conjugate of mSav*-STAR635 and biotin-PS-CFP2, we incubated both probes with a 12-fold excess of biotin-PS-CFP2 at high concentrations (> 1 mg ml^{-1}) for 2 hours at RT in 1 x PBS and purified the resulting construct PS-CFP2-mSav*-STAR635, which can bind to DGS-NTA(Ni) on SLBs, together with biotin-PS-CFP2, which cannot bind to DGS-NTA(Ni) on SLBs, via gel filtration (Superdex-200 10/30, GE Healthcare Life Sciences). Resulting peak fractions containing only the PS-CFP2-mSav*-STAR635 construct (as verified via SDS PAGE) were stored in 1 x PBS and 50 % glycerol at -20 °C.

To combine PS-CFP2* with monovalent streptavidin (mSav*) while keeping the biotin binding site unoccupied, we site-specifically conjugated PS-CFP2* with 6-Methyl-Tetrazine-PEG4-Maleimide (Jena Bioscience) and the monovalent streptavidin (mSav*) with TCO-PEG3-Maleimide (Jena Bioscience) at their free cysteines according to the manufacturer's instructions. PS-CFP2*-tetrazine and mSav*-TCO were purified from free 6-Methyl-Tetrazine-PEG4-Maleimide and TCO-PEG3-Maleimide, respectively via gel filtration (Superdex-75 10/300; GE Healthcare Life Sciences). We incubated PS-CFP2*-tetrazine with

mSav*-TCO in a 5:1 molar ratio at high concentrations (> 1 mg ml^{-1}) for 1 day at 4°C in 1 x PBS. The resulting adduct mSav*-cc-PS-CFP2* was purified together with an excess of PS-CFP2*-tetrazine via Ni-NTA based affinity chromatography (QIAGEN) and gel filtration (Superdex 200 10/30, GE Healthcare Life Sciences). Fractions containing mSav*-cc-PS-CFP2*, which can bind to biotin, as well as unreacted PS-CFP2*-tetrazine, which cannot bind to biotin, were identified via SDS PAGE, concentrated with Amicon Ultra-4 centrifugal filters (10 kDa cut-off, Merck) and stored in 1 x PBS supplemented with 50 % Glycerol at -20 °C.

The CD11a (LFA-1α chain) reactive monoclonal antibody TS2/4 (BioLegend) was conjugated with EZ-Link™ NHS-LC-LC-Biotin (Thermo Fisher Scientific) according to the manufacturer´s instructions. The mAb TS2/4-biotin was purified from an excess of NHS-LC-LC-Biotin via gel filtration (Superdex-200 10/300; GE Healthcare Life Sciences), concentrated using Amicon Ultra-4 centrifugal filters (10 kDa cut-off, Merck) and stored in 1 x PBS at 4 °C.

SDS PAGE and silver staining

Samples were mixed with a 4 x loading buffer (252 mM Tris–HCl, 40 % glycerol, 8 % SDS, and 0.04 % bromophenol blue, pH 6.8) with or without 20 mM dithiothreitol (Merck) for reducing and non-reducing conditions, respectively, and then subjected to 10 % SDS-PAGE in running buffer (25 mM Tris–HCl, 192 mM glycine and 0.1% SDS, pH 8.2) followed by silver staining as described[33].

Preparation of glass-supported lipid bilayers and fibronectin-coated surfaces

100 µg of 1,2-dipalmitoyl-*sn*-glycero-3-phosphocoline (DPPC) and 0.75 µg of 1,2-dioleoyl-*sn*-glycero-3-[*N*(5-amino-1-carboxypentyl)iminodiacetic acid] succinyl[nickel salt] (DGS-NTA(Ni); Avanti Polar Lipids) were mixed in chloroform, dried under N_2, dissolved in 1 ml PBS at 50 °C and bath-sonicated at 50 °C. Glass cover slips (#1.5, 24x60 mm, Menzel,

Germany) were plasma-cleaned for 10 minutes in an Harrick Plasma Cleaner (Harrick) and attached to 8-well LabTek chambers (Nunc, USA), for which the bottom glass slide had been removed, with two-component dental imprint silicon glue (Picodent twinsil 22, Picodent, Germany). Slides were incubated with the vesicle suspension in PBS for 10 minutes and afterwards rinsed with 1 x PBS. The histidine-tagged protein complex PS-CFP2-mSav*-STAR635 was added in concentrations yielding single molecule density, incubated for 75 minutes and rinsed with 1 x PBS. For experiments involving paraformaldehyde-based fixation, the samples were fixed with 4% paraformaldehyde (PFA; Polysciences) in 1 x PBS for 10 minutes at 25 °C and subsequently rinsed with 1 x PBS. For experiments involving glutathione (Merck) a 10 mM glutathione stock was prepared and added in a 1:1 (v/v) ratio to the sample. For T cell experiments on lipid bilayers, vesicles containing 90% 1-palmitoyl-2-oleoyl-sn-glycero-3-phosphocholine (POPC; Avanti Polar Lipids) and 10% DGS-NGA(Ni) were prepared as described [34]. 8-well LabTek chambers were modified as described above. The bilayer was functionalized by addition of His_{10}-ICAM-1 (Sinobiologicals) and incubation for 75 min.

To prepare fibronectin-coated surfaces, we incubated clean glass cover slips (glued to 8-well LabTek chambers) with 30 µg ml^{-1} fibronectin (Merck) in 1 x PBS for 2 h at 37 °C. Chambers were washed in imaging buffer (HBSS, Gibco, supplemented with 1 % FCS, 2 mM $MgCl_2$ and 2 mM $CaCl_2$) before addition of cells.

Preparation of cell samples for microscopy

The samples for CD3ζ-PS-CFP2 experiments were prepared as previously described[35]. In brief, 1 x 10^6 cells were washed and added to the sample chambers. Cells were allowed to adhere for 15 minutes, followed by fixation with 4 % PFA and 0.2 % glutaraldehyde (GA) for 10 min.

For CD11a PALM measurements, 0.3 x 10^6 CAR T cells were incubated with 3 % beriglobin (CSL Behring) for 10 minutes and subsequently stained with 40 µg ml^{-1} mAb TS2/4-biotin for 30 minutes on ice followed by a washing step in 15 ml imaging buffer (HBSS supplemented with 1 % FCS, 2 mM $MgCl_2$ and 2 mM $CaCl_2$) and a staining step employing 50 µg ml^{-1} mSav-cc-PS-CFP2 for 30 minutes on ice. After an additional washing step, cells were allowed to spread on fibronectin-coated glass slides for 10 minutes at 25 °C. After cell attachment, samples were carefully washed with 1 x PBS and fixed with 4 % PFA in 1 x PBS for 25 minutes at 4 °C. Fixation was stopped by washing the sample with 1 x PBS and imaging buffer (HBSS supplemented with 1 % FCS, 2 mM $MgCl_2$ and 2 mM $CaCl_2$). Samples were stored at 4 °C prior to imaging.

Microscopy

Objective-based TIRF microscopy was conducted using an inverted microscope (Axiovert 200, Zeiss, Germany), a chromatically corrected objective (100 x NA = 1.46, Plan-Apochromat, Zeiss, Germany) and a 405 nm (photoswitching of PS-CFP2; iBeam smart, Toptica), 488 nm (imaging of PS-CFP2; optically pumped semiconductor, Sapphire; Coherent, USA) and 647 nm (imaging of STAR635; iBeam smart, Toptica) laser. Single mSav*-STAR635 molecules were tracked using 647 nm excitation with a 100 ms time lag for at least 50 frames employing a power density of 1.5 kW cm^{-2}, followed by the PALM sequence involving 405 nm and 488 nm excitation. For determination of the mobility over longer time periods, tracking sequences were acquired using 647 nm excitation with a time lag of 500 ms over 120 frames. For photoswitching, the 405 nm laser was operated at continuous wave illumination at a power density of 20-30 W cm^{-2}. For rapid shuttering of the 488 nm laser illumination, an acousto-optical modulator was used (1205C, Isomet, USA). Two and 15 ms of illumination at ~3 kW cm^{-2} and ~0.4 kW cm^{-2}, respectively, were followed by a readout time of four ms, and a total

of 10,000 frames were recorded. Excitation light was uncoupled from emission light with the use of a dichroic mirror (zt488/640rpc; Chroma, USA). Emission was then was split by a Dual View system (Photometrics, USA) equipped with a 640dcxr dichroic mirror and HQ700/75 (both Chroma, USA) and 525/45 (Semrock, USA) emission filters. Fluorescence emission was detected with a back-illuminated EMCCD camera (iXon Ultra 897, Andor, UK).

All microscopy experiments involving cells were performed employing the described microscopy setup, illumination schemes and laser powers, i.e. 2 ms illumination time at 3 kW cm^{-2} (488nm) followed by a delay time of 4 ms for read-out, continuous 405 nm illumination at 20-30 W cm^{-2} and a sequence length of 10,000 frames.

Single Molecule Blinking Analysis

Single molecules appearing in both channels were detected and localized by using a Maximum Likelihood Estimator implemented in the ThunderSTORM ImageJ plugin[36].

To determine the mobility of mSav* on the DPPC bilayer, a published[37] algorithm implemented in MATLAB was used for the generation of trajectories, which were subjected to a mean square displacement analysis.

Independently of tracking, the position of mSav*-STAR635 molecules was averaged during the imaging period by using the localization merging algorithm implemented in ThunderSTORM with the following parameters: maximum t_{off} = 10.000 frames, maximum displacement = 1 pixel. This mean position was then employed for co-localization analysis.

Determined positions of mSav*-STAR635 were corrected for chromatic aberration by a transformation matrix, which was experimentally derived from imaging TetraSPECK beads (Thermo Fisher Scientific, USA). mSav*-STAR635 molecules with a nearest neighbor within a distance smaller than 3.5 pixels were discarded. For the remaining mSav*-STAR635 molecules PS-CFP2 signals within a radius of 1 pixel were selected for further analysis.

Simulations

A 15 x 15 µm region of interest featuring molecules at specified densities was simulated as described[35]. Briefly, a probability mask was generated by placing centers of clusters randomly according to a uniform distribution, and distributing the positions of molecules within clusters based on a two-dimensional Gaussian function located at the cluster center and truncated at the cluster size, i.e. 1 σ. A given proportion of molecules was attributed to clusters (% of molecules in cluster). Remaining molecular positions were randomly added on areas outside the clusters. To include blinking, the number of detections per label was drawn from the experimentally derived probability distribution of N. Last, signals were shifted 25 nm into a random direction, representing optimized experimental positional accuracy. For comparison with cell-associated microscopy data, the approximate expression levels of CD3ξ-PS-CFP2 and LFA-1 within a region of interest was determined by dividing the number of localizations with the mean number of detections per PS-CFP2 molecule and used for further simulations.

Code availability

Software which has been used to perform simulations is available for download. Software to analyze blinking behavior is available upon request.

Data availability

The datasets generated during and/or analyzed during the current study are available from the corresponding authors upon request.

CONTRIBUTIONS

RP, GJS, JBH and MB conceived the project. BKR, RP, GJS, JBH and MB wrote the manuscript. RP developed the linker system. contributed all probes and performed imaging experiments. MB analyzed data. BKR performed imaging experiments, analyzed data and developed software tools. ES, FB and HS contributed important ideas.

ACKNOLEDGEMENTS

This work was supported by the Austrian Science Fund (FWF) through the PhD program Cell Communication in Health and Disease W1205 (JBH and HS), the projects I953-B20 (MB), V538-B26 (ES), P27941-B28 (FB), P26337-B21, P 25730-B21, P 30214-N36 (GJS), P 25775-B2 (JBH) and the Vienna Science and Technology Fund (WWTF) projects LS13-030 (GJS, JBH). Funding was further provided by a predoctoral fellowship from the Boehringer Ingelheim Fonds (RP).

REFERENCES

1. Betzig, E. *et al.* Imaging Intracellular Fluorescent Proteins at Nanometer Resolution. *Science* **313**, 1642-1645 (2006).

2. Hess, S.T., Girirajan, T.P. & Mason, M.D. Ultra-high resolution imaging by fluorescence photoactivation localization microscopy. *Biophys J* **91**, 4258-4272 (2006).

3. Ando, R., Hama, H., Yamamoto-Hino, M., Mizuno, H. & Miyawaki, A. An optical marker based on the UV-induced green-to-red photoconversion of a fluorescent protein. *Proc Natl Acad Sci U S A* **99**, 12651-12656 (2002).

4. Subach, F.V. *et al.* Photoactivatable mCherry for high-resolution two-color fluorescence microscopy. *Nat Methods* **6**, 153-159 (2009).

5. Wiedenmann, J. *et al.* EosFP, a fluorescent marker protein with UV-inducible green-to-red fluorescence conversion. *Proc Natl Acad Sci U S A* **101**, 15905-15910 (2004).

6. Ando, R., Mizuno, H. & Miyasaka, M. Regulated Fast Nucleocytoplasmic Shuttling Observed by Reversible Protein Highlighting. *Science* **306**, 1370-1373 (2004).

7. Patterson, G. & Lippincott-Schwartz, J. A Photoactivatable GFP for Selective Photolabeling of Proteins and Cells. *Science* **297**, 1873-1877 (2002).

8. Chudakov, D.M. *et al.* Photoswitchable cyan fluorescent protein for protein tracking. *Nat Biotech* **22**, 1435-1439 (2004).

9. Chudakov, D.M., Lukyanov, S. & Lukyanov, K.A. Tracking intracellular protein movements using photoswitchable fluorescent proteins PS-CFP2 and Dendra2. *Nat. Protocols* **2**, 2024-2032 (2007).

10. Chudakov, D.M., Matz, M.V., Lukyanov, S. & Lukyanov, K.A. Fluorescent Proteins and Their Applications in Imaging Living Cells and Tissues. *Physiological Reviews* **90**, 1103-1163 (2010).

11. Smith, C.S., Joseph, N., Rieger, B. & Lidke, K.A. Fast, single-molecule localization that achieves theoretically minimum uncertainty. *Nat Methods* **7**, 373-375 (2010).

12. Annibale, P., Vanni, S., Scarselli, M., Rothlisberger, U. & Radenovic, A. Identification of clustering artifacts in photoactivated localization microscopy. *Nat Methods* **8**, 527-528 (2011).

13. Annibale, P., Scarselli, M., Kodiyan, A. & Radenovic, A. Photoactivatable Fluorescent Protein mEos2 Displays Repeated Photoactivation after a Long-Lived Dark State in the Red Photoconverted Form. *J Phys Chem Let* **1**, 1506-1510 (2010).

14. Rossy, J., Owen, D.M., Williamson, D.J., Yang, Z. & Gaus, K. Conformational states of the kinase Lck regulate clustering in early T cell signaling. *Nat Immunol* **14**, 82-89 (2013).

15. Lillemeier, B.F. *et al.* TCR and Lat are expressed on separate protein islands on T cell membranes and concatenate during activation. *Nat Immunol* **11**, 90-96 (2010).

16. Wang, S., Moffitt, J.R., Dempsey, G.T., Sunney Xie, X. & Zhuang, X. Characterization and development of photoactivatable fluorescent proteins for single-molecule-based superresolution imaging. *Proc Natl Acad Sci U S A* **111**, 8452-8457 (2014).

17. Sengupta, P. & Lippincott-Schwartz, J. Quantitative analysis of photoactivated localization microscopy (PALM) datasets using pair-correlation analysis. *BioEssays : news and reviews in molecular, cellular and developmental biology* **34**, 396-405 (2012).

18. Annibale, P., Vanni, S., Scarselli, M., Rothlisberger, U. & Radenovic, A. Quantitative photo activated localization microscopy: unraveling the effects of photoblinking. *PLoS One* **6**, e22678 (2011).

19. Lee, S.-H., Shin, J.Y., Lee, A. & Bustamante, C. Counting single photoactivatable fluorescent molecules by photoactivated localization microscopy (PALM). *Proceedings of the National Academy of Sciences* **109**, 17436-17441 (2012).

20. Nieuwenhuizen, R.P. *et al.* Quantitative localization microscopy: effects of photophysics and labeling stoichiometry. *PLoS One* **10**, e0127989 (2015).

21. Tamm, L.K. & McConnell, H.M. Supported phospholipid bilayers. *Biophys J* **47**, 105-113 (1985).

22. Hughes, L.D., Rawle, R.J. & Boxer, S.G. Choose your label wisely: water-soluble fluorophores often interact with lipid bilayers. *PLoS One* **9**, e87649 (2014).

23. Pageon, S.V. *et al.* Functional role of T-cell receptor nanoclusters in signal initiation and antigen discrimination. *Proc Natl Acad Sci U S A* **113**, E5454-5463 (2016).

24. Montero, D., Tachibana, C., Rahr Winther, J. & Appenzeller-Herzog, C. Intracellular glutathione pools are heterogeneously concentrated. *Redox Biol* **1**, 508-513 (2013).

25. Kiskowski, M.A., Hancock, J.F. & Kenworthy, A.K. On the use of Ripley's K-function and its derivatives to analyze domain size. *Biophys J* **97**, 1095-1103 (2009).

26. Baumgart, F. *et al.* Varying label density allows artifact-free analysis of membrane-protein nanoclusters. *Nat Methods* (2016).

27. Cambi, A. *et al.* Organization of the integrin LFA-1 in nanoclusters regulates its activity. *Molecular biology of the cell* **17**, 4270-4281 (2006).

28. Baumgart, F., Arnold, A.M., Rossboth, B.K., Brameshuber, M. & Schutz, G.J. What we talk about when we talk about nanoclusters. *Methods Appl Fluoresc* **7**, 013001 (2018).

29. Spahn, C., Herrmannsdorfer, F., Kuner, T. & Heilemann, M. Temporal accumulation analysis provides simplified artifact-free analysis of membrane-protein nanoclusters. *Nat Methods* **13**, 963-964 (2016).

30. Huppa, J., Gleimer, M., Sumen, C. & Davis, M. Continuous T cell receptor signaling required for synapse maintenance and full effector potential. *Nature immunology* **4**, 749-755 (2003).

31. Fairhead, M., Krndija, D., Lowe, E.D. & Howarth, M. Plug-and-play pairing via defined divalent streptavidins. *J Mol Biol* **426**, 199-214 (2014).

32. Howarth, M. *et al.* A monovalent streptavidin with a single femtomolar biotin binding site. *Nature methods* **3**, 267-273 (2006).

33. Chevallet, M., Luche, S. & Rabilloud, T. Silver staining of proteins in polyacrylamide gels. *Nat. Protocols* **1**, 1852-1858 (2006).

34. Huppa, J.B. *et al.* TCR-peptide-MHC interactions in situ show accelerated kinetics and increased affinity. *Nature* **463**, 963-967 (2010).

35. Rossboth, B. *et al.* TCRs are randomly distributed on the plasma membrane of resting antigen-experienced T cells. *Nat Immunol* **19**, 821-827 (2018).

36. Ovesny, M., Krizek, P., Borkovec, J., Svindrych, Z. & Hagen, G.M. ThunderSTORM: a comprehensive ImageJ plug-in for PALM and STORM data analysis and super-resolution imaging. *Bioinformatics* **30**, 2389-2390 (2014).

37. Gao, Y. & Kilfoil, M.L. Accurate detection and complete tracking of large populations of features in three dimensions. *Optical Express* **17**, 4685-4704 (2009).